RESEARCH ARTICLE

Effect of Soil Salt Content on Stray Current Corrosion of Buried Metal

YANING LI[ID][1]**, MENG JIAO**[ID][1]**, YE WANG**[2]**, WENFEI LI**[1]**, HONG KANG**[1]**, AND WENCAI ZHANG**[1]

[1]School of Automation and Electrical Engineering, Lanzhou Jiaotong University, Lanzhou 730070, China
[2]School of Environmental and Municipal Engineering, Lanzhou Jiaotong University, Lanzhou 730070, China

Corresponding authors: Yaning Li (liyaning@mail.lzjtu.cn) and Ye Wang (wy72000@163.com)

ABSTRACT In order to study the effect of soil salt content on the corrosion of buried metal by the stray current in urban rail transit, a small experimental platform for the buried metal corrosion is built. The corrosion rate and mass loss of buried carbon steel specimens in soil samples with or without DC stray current are measured and calculated when different content of NaCl is added into the soil samples, respectively. The experimental results show that the corrosion rate and mass loss of the buried metal increase with the increase of soil salt content. DC stray current will aggravate the corrosion of the buried metal. The corrosion degree of buried metal will be seriously aggravated under the coupling action of DC stray current and salt. When there is no DC stray curren, the corrosion degree of buried metal is relatively small, and the influence of soil salt content on the buried metal corrosion is also relatively small. Finally, a multiphysics simulation model corresponding to the experiment is established to verify the experimental results. The simulation results are basically consistent with the experimental results, which proves the accuracy of the experimental results. The research results can provide a theoretical basis for the corrosion protection design of subway stray current.

INDEX TERMS Corrosion, multiphysics simulation, salt content, stray current, urban rail transit.

I. INTRODUCTION

In recent years, urban rail transit has shown a large-scale and high-speed development trend with its outstanding advantages of fastness, efficiency, and safety. It has become an important part of urban transportation and has played an important role in improving the urban transportation environment [1]. However, with the rapid development and long-term operation of urban rail transit, the accompanying stray current problem cannot be ignored. Electrochemical corrosion will occur when the stray current flows through reinforced concrete, metal equipment and other buried metal pipes near the line, which will cause corrosion perforation, shortened service life, gas leakage and other problems, resulting in huge economic losses, potential safety hazards, and so on [2]–[5]. Therefore, studying the influencing factors

The associate editor coordinating the review of this manuscript and approving it for publication was Jesus Felez[ID].

of buried metal corrosion in the presence of DC stray current can provide a theoretical basis for the design of stray current corrosion protection, and it is of great significance to ensure the long-term safe operation of urban rail transit and the protection of buried metals.

Since the appearance of subway, most countries in the world have attached great importance to the protection and impact evaluation of subway stray current, and many scholars have carried out a lot of research. At present, the related research mainly focuses on the stray current distribution and its influencing factors, and the corrosion of buried metal caused by stray current. Many studies have proposed models for predicting stray current distribution in DC electrified railway systems based on various principles, such as a simulation model of stray current in long line based on CDEGS software [6], a calculation method of stray current based on infinitesimal algorithm in the case of multiple power supply sections [7]. And the surface potential gradient around

the subway line is calculated and measured based on the finite element method, and the corrosion range of stray current is determined [8]. Besides, a large number of studies show that the magnitude and distribution of stray currents are affected by many factors, such as rail-to-ground transition resistance, vehicle operating conditions, rail longitudinal resistance, train traction current, system resistivity, and the distance between traction substations [9]–[13].

In addition, various models are established to analyze the law and trend of the buried metal corrosion caused by the stray current. For example, by establishing a multi-physical finite element model of DC metro traction system, the dynamic process of the buried pipeline corrosion caused by stray current is calculated, and the corrosion rate change and corrosion trend of stray current are analyzed [14]. By establishing a segment corrosion calculation model including the track bed structure, the reinforcement corrosion problem caused by DC stray current in the cracked section of the shield tunnel is studied, and the potential distribution and reinforcement corrosion law in the cracked section under different input and output positions are obtained [15]. Based on a mathematical method combined with finite element model and experimental analysis, the pipeline-soil potential under the interference of the track stray current is calculated, and the change law of electrochemical corrosion of metal pipelines is studied [16]. The influence of the geometrical position of the steel bars on the corrosion of the steel bars under the action of stray current is studied, and the results show that the corrosion state of the steel bars parallel to the current direction is more obvious and more likely to cause local corrosion [17]. The influence factors of DC stray current on the corrosion of the carbon steel are analyzed. For example, the influence of DC stray current on the corrosion of low carbon steel and 10% Cr steel in saturated Ca(OH)2 solution is studied through experiments and the results show that DC stray current aggravates the corrosion degree of carbon steel [18]. The coupling effect of chloride ion and DC stray current on the soil corrosion of three grounding grid materials is studied and the results show that both chloride ion and DC stray current will accelerate the corrosion rate of grounding grid materials [19]. The different effects of stray current and anodic polarization on the corrosion of the steel bars in mortar are verified by experiments and it is found that the electrochemical performance of steel bars caused by anodic polarization is significantly different from that of stray current under the same conditions in all studies [20]. Many scholars have also proposed evaluation and prediction models for stray current corrosion. For example, a comprehensive model for evaluating the remaining life of corroded gas pipelines is proposed for the risk of pipeline failure under impac of the stray current [21]. Based on nonlinear finite element analysis and artificial neural network model, a new failure pressure prediction method for high-strength steel pipe containing stray current corrosion defects is proposed [22]. A numerical simulation algorithm based on the finite element is proposed to analyze the influence of stray current corrosion

on the high-speed rail transit viaduct, and the effectiveness of numerical simulation algorithm to calculate stray current field distribution is verified [23]. Based on the research of stray current corrosion at home and abroad, the main sources, formation causes and corrosion hazards of stray current are introduced from DC and AC stray current respectively, and the corrosion characteristics, corrosion rate difference and corrosion mechanism of them are systematically discussed and summarized [24]. Besides, Some scholars have studied the corrosion resistance of different steel materials to stray current. For example, an experimental study is conducted on the corrosion of the rock bolts by simulating stray current input and monitoring polarization potential, and the results show that the bonded wire is more resistant to stray current corrosion than HRB500 steel bars [25].

Through the analysis of the research status of a large number of the stray current and corrosion problems, it can be found that calculation and prediction models of stray current distribution in DC electrified railway system based on various principles are proposed. Or the influencing factors of the stray current are studied. Besides, the law and the influencing factors of the buried metal corrosion caused by the stray current have been studied, and the evaluation and prediction models of the buried metal corrosion by the stray current have been proposed, so as to provide a theoretical basis for preventing the corrosion of buried metal. However, there is little research on the effect of soil physical and chemical properties on the buried metal corrosion in the presence of stray current in urban rail transit. Therefore, this paper mainly studies the effect of soil salt content on the corrosion of buried metal in the presence of stray current, in order to provide reference for the corrosion protection design of subway stray current.

II. STRAY CURRENT CORROSION MECHANISM

The DC traction power supply system of urban rail transit supplies power to trains through the traction network or the third rail, and uses the running rail to return. However, due to the limitations of the operating environment, technical conditions and other factors, the running rail cannot be absolutely insulated from the ground, which cause a part of the return current to leak from the running rail, and form stray current. And the buried pipelines and metal structures are corroded by the stray current. The schematic diagram of stray current generation is as shown in Fig. 1.

When the stray current leaking to the soil flows through the buried metal, it will cause the electrochemical reaction of the buried metal. The metal anode area will occur oxidation reaction, and the buried metal will lose electrons and become ferrous ions:

$$Fe - 2e^- \rightarrow Fe^{2+} \tag{1}$$

The ions Fe^{2+} generated in the anode area of the metal will further react to form $Fe(OH)_2$ and $Fe(OH)_3$ and precipitate from the buried metal surface. Some products will react with
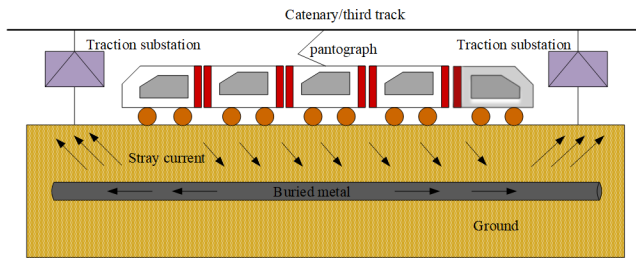
**FIGURE 1.** Schematic diagram of stray current generation.

water and oxygen to form $Fe_2O_3 \cdot H_2O$ (red rust) and Fe_3O_4 (black rust). Besides, the reduction reaction will occur in the metal cathode region, and the reaction type is related to the pH value and oxygen content of the soil environment. The hydrogen evolution reaction occurs when the soil around the buried pipeline is acidic:

$$2H^+ + 2e^- \rightarrow H_2 \uparrow \qquad (2)$$
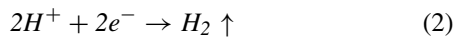
When buried metals are in neutral or alkaline soil environment and oxygen is present, oxygen absorption reaction will occur:

$$O_2 + 2H_2O + 4e^- \rightarrow 4OH^- \qquad (3)$$
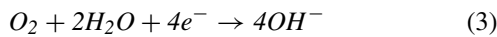
When in an oxygen-free environment, the hydrolysis reaction will occur in the buried metal cathode region:

$$2H_2O + 2e^- \rightarrow H_2 \uparrow +2OH^- \qquad (4)$$
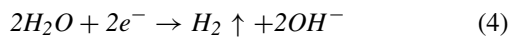
According to Faraday's law of electrical corrosion, the corrosion mass M of metal can be expressed as:

$$M = K \cdot J \cdot t \qquad (5)$$

where, M is the corrosion mass per unit area of the metal, g/m^2; K is the electrochemical equivalent of the metal, $g/(A \cdot h)$; J is the current density, A/m^2; t is the time, h.

III. CORROSION EXPERIMENT OF BURIED METAL BY STRAY CURRENT

A. EXPERIMENTAL SAMPLES AND EQUIPMENT

The corrosion experiment of soil salt content on stray current buried metals is set up in the laboratory. The schematic diagram of the experiment is shown in Fig. 2. In the Fig. 2, the size of the container for placing the soil is 25.5*16*15.5 cm, and the height of soil filling is 12cm, that is, the size of the soil part embedded in the box is 25.5*16*12 cm. Buried in the soil is Q345 carbon steel sheet with a size of 9*5*0.08 cm, as shown in Fig. 3. The carbon steel test piece is located in the middle of the horizontal plane with a buried depth of 8 cm (the depth of the box is 11.5 cm). Carbon rods with a diameter of 5 mm and a length of 5 cm are used as positive and negative electrodes to conduct electricity. The carbon rods are located in the middle of 2.5cm away from the soil boundary, that is, the distance between the positive and negative carbon rods is 10.4cm. The depth of the carbon rod inserted into the soil is 2 cm, that is, 3cm is left outside the soil to connect the

positive and negative poles of the power supply. The Faithtech FT10010 linear DC power supply is used to simulate the traction substation. Its output voltage scope is 0 ~100 V, and the output current scope is 0 ~10 A, and the resolution is 100 mV and 100 mA respectively. The instrument used to measure soil salt content is TPY-8A soil nutrient rapid tester, which can measure soil salt content in the range of 0~23 mS/cm with an accuracy of ±2% FS. The instrument used to measure the weight of the steel sheet is the type of AB104~S/FA electronic analytical balance with readability of 0.0001 g. The NaCl reagent is used to adjust the soil salt content.

The type of soil used in the experiment is loam. First, the soil is retrieved from the vicinity of the subway station, and the obtained soil is filtered by a sieve with a diameter of 43 cm and an aperture of 4 mm, so as to filter out sundries such as stones, weeds and roots in the soil. Then, an appropriate amount of distilled water is evenly added into the soil sample, and it is allowed to stand for about 10 days until the added distilled water penetrates into the soil evenly. Finally, filter it again through with a sieve with a diameter of 43 cm and an aperture of 2.5 mm. So the soil sample is prepared.
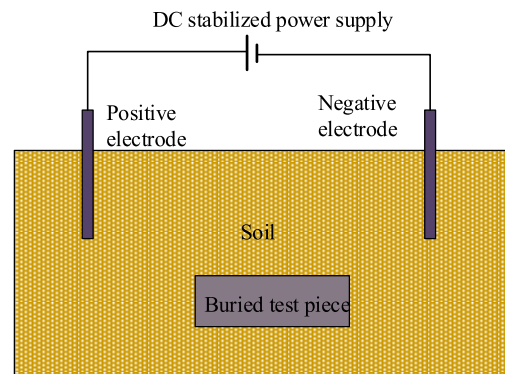

FIGURE 2. Schematic diagram of the experiment.

FIGURE 3. Carbon steel test piece.

B. EXPERIMENTAL METHOD AND STEPS

After the treatment, the soil samples are divided into 8 equal parts, and 4 parts are used to the experimental group and the other 4 parts are the control group. In the experiment

TABLE 1. Experimental sample parameters.

Number	NaCl content	Soil conductivity (mS/cm)	Soil Humidity (%)	Soil temperature (°C)	Soil compaction (N/cm^2)	steel sheet weight (g)	Buried depth of steel (cm)
1	0	0.03	7.4	20.2	3.37	31.3659	8
2	10	3.23	7.6	20.3	3.37	31.3655	8
3	20	6.39	7.4	20.2	3.37	31.3653	8
4	30	10.21	7.5	20.3	3.37	31.3552	8
5	0	0.03	7.4	20.1	3.37	31.3558	8
6	10	3.25	7.5	20.4	3.37	31.3621	8
7	20	6.41	7.6	20.3	3.37	31.3657	8
8	30	10.18	7.4	20.2	3.37	31.3596	8

group, the first soil sample is not added with NaCl, and its salt content, conductivity, temperature, humidity, and compactness of the soil sample are measured by the related sensors of the soil nutrient rapid tester. These parameters are measured because they will have an effect on the experimental results. Therefore, in order to ensure the accuracy of the experimental results, it is necessary to control these parameters to be the same, so as to study the influence of soil salt content on buried metal corrosion caused by stray current in urban rail transit. In addition, the PH of the soil sample also has an effect on the corrosion of the buried test pieces. However, as NaCl reagent is added to the soil, which is neutral, the subsequent verification shows that adding NaCl reagent will not affect the PH of the soil samples, so the soil PH is not measured.

After the measurement of related parameters is completed, The No.1 carbon steel sheet is buried in the soil with a depth of 8 cm. Then the 10g NaCl is added into the second soil sample, and stirred evenly, and its relevant parameters are measured by the soil nutrient rapid tester. Then, the No.2 carbon steel sheet is buried in the soil with a depth of 8 cm. 20g and 30g NaCl is added into the third and fourth soil samples respectively, and the previous steps are repeat, and the carbon steel sheets are numbered as 3 and 4 respectively. The salt content of the four soil samples in the control group and the buried depth of carbon steel sheets are exactly same as the four samples in the experimental group, and the carbon steel pieces are numbered 5, 6, 7 and 8 in sequence. The parameters of each soil sample and the carbon steel sheet mass are shown in Table 1. The salt content of soil in the experiment is designed according to reference [26], [27].

After the experimental samples are made, the four soil samples in the experimental group are supplied with DC current respectively, and the voltage of the DC power supply are adjusted to 30 V. Graphite electrodes are connected to the positive and negative electrodes of the power supply to conduct electricity respectively. At the same time, the control group is placed indoors for corrosion test. The experimental period is 30 days, with 15 hours of electricity per day. The experimental device is shown in Fig. 4. After the end of the experiment period, the carbon steel sheets buried in the soil are taken out for post-treatment such as polishing, cleaning and blow-drying. The corrosion morphology of the carbon steel sheets in each experimental sample is observed, and the

corrosion mass loss of the carbon steel sheets is measured and the corrosion rate is calculated.

C. EXPERIMENTAL RESULTS AND ANALYSIS

After the end of the experiment period, the carbon steel sheets in each soil sample are post-treated, and the corrosion morphology of the buried carbon steel sheets is shown in Fig. 5. It can be seen from the figure that the corrosion degree of the carbon steel sheet is small in the control experiment (numbered 5∼8), and the corrosion area is relatively uniform, and with the increase of the soil salt content, the corrosion of the carbon steel sheet is more serious. Under the same conditions, the carbon steel sheets in the experimental group (numbered 1∼4) are severely corroded, and the corrosion area is uneven. The anode of the carbon steel sheet is severely corroded, and the thickness of the carbon steel sheet is obviously thinned and deformed, while the cathode is slightly corroded. Besides, with the increase of soil salt content, the corrosion of carbon steel sheet becomes more and more serious. When 30 g NaCl is added to the soil and electrified, the deformation of carbon steel sheet is obvious(No. 4), and even it has the perforation phenomenon.

The corrosion mass loss and the corrosion rate of each carbon steel sheet is weighted and calculated, as shown in Table 2. It can be seen from the Table 2 that when the NaCl content is 0 g, 10 g, 20 g, and 30 g, the mass loss of the carbon steel sheet in the experimental group is 1.5531 g, 2.4432 g, 3.4957 g and 5.7119 g, respectively, while that in the control group is 0.0112g, 0.5516g, 0.6426g, and 1.1505g respectively. Through the analysis of the corrosion rate in the Table 2, it can be found that when the DC current is applied, the corrosion rate of carbon steel sheet with soil salt content of 10 g, 20 g and 30g is 1.57 times, 2.25 times and 3.68 times of that without NaCl, respectively. It shows that the corrosion mass loss and the corrosion rate of the carbon steel sheet increase with the increase of soil salt content.

The change trend of the mass loss of the experimental group and the control group corresponding to different soil salt content is shown in Fig. 6. It can be seen from the figure that both in the control group and the experimental group, the mass loss of the carbon steel sheets increases with the increase of soil salt content. Therefore, the soil salt content will aggravate the corrosion of the buried metals. When DC power supply is applied, the corrosion mass loss of carbon steel specimen is obviously increased compared with that

TABLE 2. Experimental results.

Number	Pre-test mass (g)	Post-test mass (g)	Mass loss (g)	Corrosion rate (g/day)	Percent of mass loss
1	31.3659	29.8128	1.5531	0.05177	4.95%
2	31.3655	28.9223	2.4432	0.08144	7.79%
3	31.3653	27.8696	3.4957	0.11652	11.15%
4	31.3552	25.6433	5.7119	0.19040	18.22%
5	31.3558	31.3446	0.0112	0.00037	0.04%
6	31.3621	30.8105	0.5516	0.01839	1.76%
7	31.3657	30.7231	0.6426	0.02142	2.05%
8	31.3596	30.2091	1.1505	0.03835	3.67%

(a) Experimental group
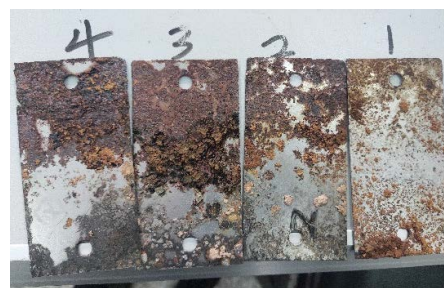
(b) Control group

FIGURE 4. Experimental device.

(a) Experimental group

(b) Control group

FIGURE 5. Corrosion morphology of carbon steel sheet.

without power supply. So, the carbon steel specimens will be more seriously corroded under the coupling effect of current and NaCL. In addition, it also can be seen from the figure that the corrosion mass loss of carbon steel sheet in the experimental group changes more obviously with the increase of soil salt content, while the change in the control group is relatively gentle. It is concluded that the applied current will increase the influence of soil salt content on the buried metal corrosion.

IV. MULTIPHYSICS SIMULATION MODLE
A. GEOMETRIC MODEL
The COMSOL multiphysics software is used for simulation. According to the experimental model, the simulation model of DC stray current on buried metal corrosion is established, including soil, buried carbon steel sheet and applied potential. The size of the box and buried carbon steel sheets used in the simulation model is the same as that in the experiment, that

is, the size of the container is 25.5*16*15.5 cm, and the size of the carbon steel plate is 9 * 5 * 0.08 cm. In the experiment, carbon rods are used as positive and negative electrodes to conduct electricity, but in the simulation, voltage is applied by setting the boundary electrolyte potential. Under the above conditions, a stray current distribution field is formed in the soil, which provides an electrochemical corrosion environment for buried pipeline metals.

B. THEORETICAL BASIS OF RELEVANT PHYSICS FIELDS
Two physical fields, secondary current distribution and deformation geometry, are used in the simulation. The secondary current distribution is used to study the corrosion of buried carbon steel sheet by stray current, and the deformation geometry is used to study the corrosion deformation degree of buried steel sheet. When the stray current leaks into the soil, it will change the current density distribution of the soil. Assuming the current density distributed in the
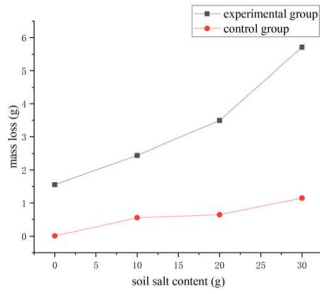
FIGURE 6. The change trend of the mass loss.

soil (electrolyte) is i_l, according to Ohm's law, it can be expressed as:

$$\nabla \cdot i_l = Q_l \tag{6}$$
$$i_l = -\sigma_l \nabla \phi_l \tag{7}$$

where, i_l is the current density in the soil, and Q_l is the current source in the soil, taking a value of 0, and σ_l is the conductivity of the soil, and ϕ_l is the potential in the soil.

When the buried carbon steel sheet in the soil environment with stray current distribution, some stray currents will flow through the buried carbon steel sheet, so the current density distributed on the carbon steel sheet i_{Fe} can be expressed as:

$$i_{Fe} = \boldsymbol{n}i_l \tag{8}$$

where, $\boldsymbol{n}$ is normal vector. The anode reaction of the buried carbon steel sheet is affected by the corrosion current density i_{loc}, and the relationship between i_{loc} and the current density flowing through the steel sheet i_{Fe} can be expressed as:

$$i_{Fe} = \sum i_{loc} \tag{9}$$

The electrode reaction speed of the buried carbon steel sheet can be expressed by the linear Butler-Volmer equation of electrode dynamics:

$$i_{loc} = i_0 \left(\frac{(\alpha_a + \alpha_c) F}{RT} \right) \eta \tag{10}$$

where, i_0 is the exchange current density of the carbon steel sheet reaction, and α_a is the anode transfer coefficient, and α_c is the cathode transfer coefficient, and F is the Faraday constant, and R is the general gas constant, and T is the temperature. η is the overpotential at the interface between the electrode and electrolyte. Due to the current distribution and self-resistance of the buried steel sheet, there is a metal electrode potential in the steel sheet, so η can be expressed as:

$$\eta = \phi_s - \phi_l - E_{eq} \tag{11}$$

where, E_{eq} is equilibrium potential of metal electrodes.

According to Faraday's law, the corrosion rate of buried pipelines (iron) can be expressed as:

$$v_{cor} = \frac{M}{nF} i_{Fe} \tag{12}$$

where, M is the average molar mass of iron, and n is the number of electrons lost by the iron reaction, and v_{corc} is the corrosion rate of the metal. After the corrosion rate of buried steel sheet is obtained, the corrosion mass loss of buried steel sheet is obtained according to the corrosion time.

C. PHYSICS SETUP AND MESHING

According to the experimental data and the theoretical basis of corrosion, the physical fields involved in the simulation are set, and the parameters and values used in the simulation are shown in Table 3. The most important part of the simulation model is the setting of the secondary current distribution physical field, which mainly includes electrolyte, insulation and electrode. The setting of the electrolyte is mainly the conductivity. In this paper, it is set according to the soil conductivity measured in the experiment. The insulation boundary is the six sides of the box. The most important setting part is the electrode surface, because corrosion occurs on the electrode surface, the reaction principle of the electrode surface is as described in the part of V.B, and the relevant parameter are shown in Table 3. In addition, two boundary electrolyte potentials are set to simulate the current source in the experiment, and the positive electrode is set to 30 V and the negative electrode is set to 0 V.

TABLE 3. Simulation parameters.

Parameters	Value	Unit	Description
σ_l	0.03	S/m	Electrolyte conductivity of the soil
σ_s	1E7	S/m	Electrolyte conductivity of the carbon steel
ϕ_{bond}	30	V	Boundary Electrolyte Potential
M	56	g/mol	Average molar mass of iron
ρ	7.8	g/cm³	Density of iron
n	2		Iron electrons lost
m	-1		Electrochemical Equivalent Coefficient
E_{eq}	-0.76	V	Iron Equilibrium Potential
i_0	7.1E-5	A/m²	Exchange current density of iron
α_a	1.5		Anode transfer coefficient
α_c	0.5		Cathode transfer coefficient
c	10		Hardening factor
F	96485	C/mol	Faraday constant

After the physical field is set up, mesh generation is carried out. Meshing generation is an important part of the simulation calculation accuracy. In order to solve the corrosion rate and the mass loss of the buried carbon steel sheet accurately, the simulation model is meshed by mapping and sweeping methods, and the adaptive meshing method is used in the solution process. This means that in the simulation process, as the interface moves, the mesh is updated to keep the mesh refined in the interface area. The grid division result is shown in Fig. 7.
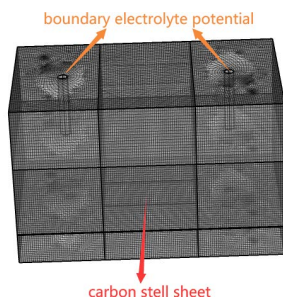
FIGURE 7. Meshing result.

V. SIMULATION RESULTS AND EXPERIMENTAL VERIFICATION

A. EXPERIMENTAI GROUP SIMULATION

After the simulation model is established, the boundary electrolyte potential is set at 30V, and the parameters in the simulation are adjusted in turn according to the experimental parameters in the experimental group for simulation verification. First, the first group of experiments is verified, that is, the stray current corrosion experiment without NaCl in the soil sample. The soil conductivity is 0.03 S/m, and the potential distribution in the soil can be obtained after calculation, as shown in Fig. 8. It can be seen from the Fig. 8 that the boundary electrolyte potential is 30 V for the positive electrode and 0 V for the negative electrode. Fig. 9 shows the vector diagram of current density in the soil, and it can be seen that the currents flow from the positive electrode to the negative electrode through the soil and the buried carbon steel sheet, but most of the currents flow through the buried carbon steel sheet and finally returns to the negative electrode.

Fig. 10 shows the corrosion rate of the buried carbon steel sheets when 0 g, 10 g, 20 g and 30 g NaCl is added to the soil samples, respectively. It can be seen from the figure that when no NaCl is added to the soil, the corrosion rate of the buried carbon steel sheet is small, and the maximum value is 3.9 $g/\left(m^2 \cdot h\right)$. When 10 g, 20 g and 30 g NaCl is added, the maximum corrosion rate reaches 5.74 $g/\left(m^2 \cdot h\right)$, 5.76 $g/\left(m^2 \cdot h\right)$ and 5.77 $g/\left(m^2 \cdot h\right)$, respectively. This indicates that the corrosion rate of carbon steel sheet increases with the increase of salt content in the soil. Moreover, it can also be seen that the buried carbon steel sheets have obvious uneven corrosion phenomenon. Serious corrosion occurred at one end, while basically no corrosion occurred at the other end, and the corrosion mainly occurs in the current outflow area, that is, the anode area near the negative electrode, which is consistent with the experimental results.

B. CONTROL GROUP SIMULATION

On the basis of the established simulation model, no boundary potential is set, that is, no external power supply to affect the corrosion of the buried carbon steel sheet. Then, the parameters in the simulation are adjusted in turn according
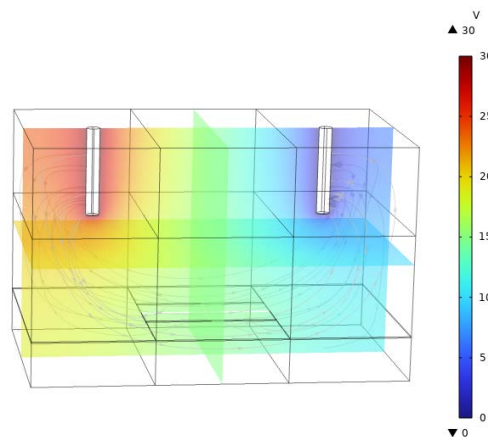

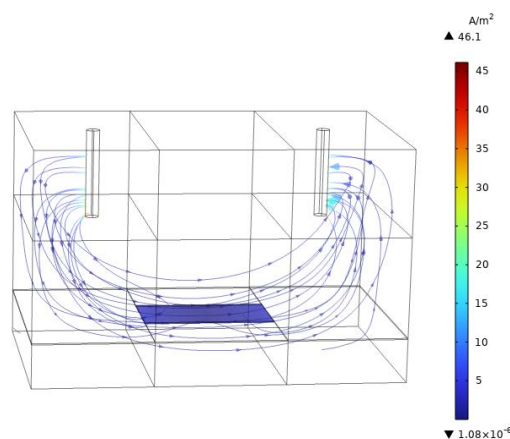**FIGURE 8.** Potential distribution in the soil.

FIGURE 9. Vector diagram of current density in the soil.

to the experimental parameters in the control group to carry out simulation verification. Fig. 11 shows the corrosion rate of the buried carbon steel sheets when 0 g, 10 g, 20 g and 30 g NaCl is added to the soil samples, respectively. It can be seen from the figure that the corrosion rate of buried carbon steel test pieces is extremely small when no salt is added into the soil, and the maximum value is only $2.75 \times 10^{-16} \times 10^{-16}$ $g/\left(m^2 \cdot h\right)$. When 10 g NaCl is added to the soil, the corrosion rate is still very small and almost unchanged. However, when the NaCl added to the soil samples reaches 20 g and 30 g, the corrosion rate changes slightly, and the maximum value is $5.51 \times 10^{-16} \times 10^{-16}$ $g/\left(m^2 \cdot h\right)$ and $2.75 \times 10^{-15} \times 10^{-16}$ $g/\left(m^2 \cdot h\right)$. It indicates that the corrosion rate of the carbon steel sheets increases with the increase of soil salt content, but the corrosion rate is very small in the absence of external power interference.

C. EXPERIMENTAL VERIFICATION AND DISCUSSION

When 10 g and 30 g NaCl is added to the soil samples, under the condition of external power supply, the comparison between simulation and experiment results is shown in
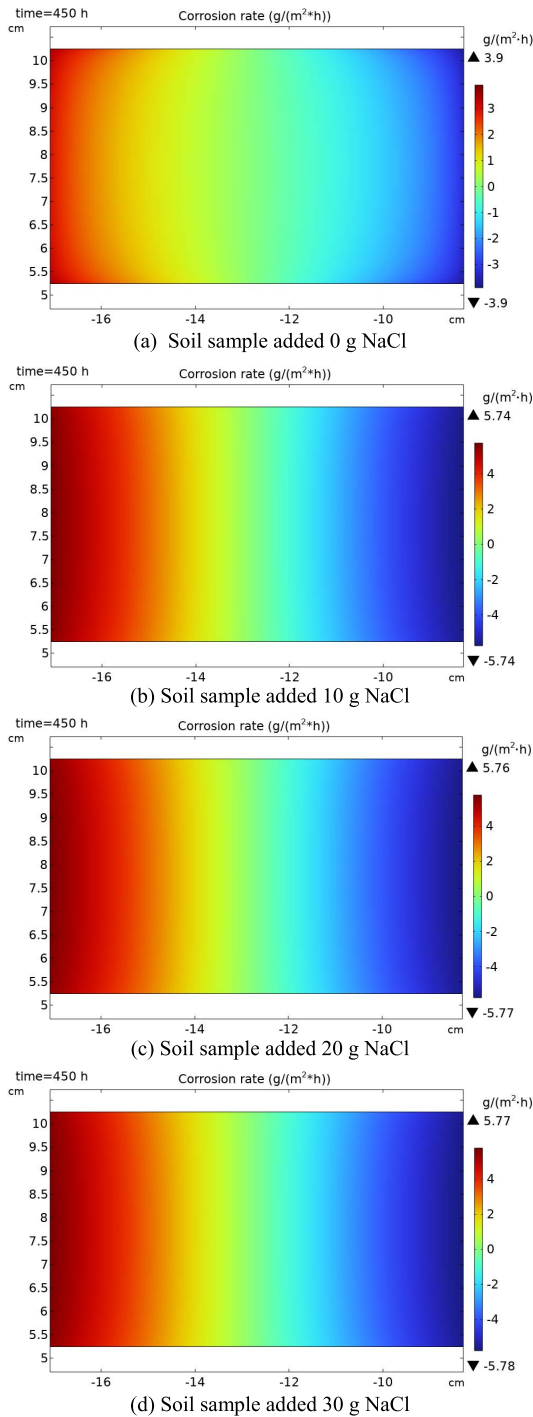
FIGURE 10. Corrosion rate simulation of experimental group.

FIGURE 11. Corrosion rate simulation of control group.

Fig. 12. It can be seen from the figure that obvious uneven corrosion occurs when an external power supply exists. In other words, obvious corrosion occurs in the anode area. Even when 30g NaCl is added to the soil, the carbon steel specimen is obviously thinned and perforated, while almost no corrosion occurs in the cathode area. In addition, through the analysis of the experimental results, it can be found that the corrosion degree and corrosion rate of the carbon steel sheets increase with the increase of soil salt content.

Under the condition of no external power supply, when 0 g and 20 g NaCl is added to the soil samples, the comparison of simulation and experiment results is shown in Fig. 13. It can be seen from the figure that the corrosion of the carbon steel sheets is relatively uniform, and there is no obvious local
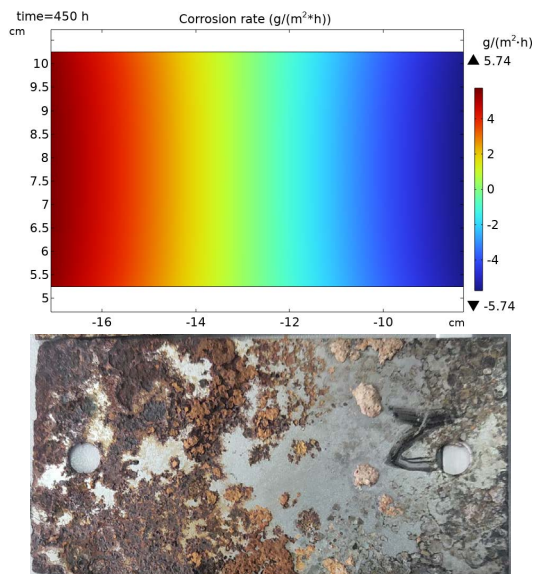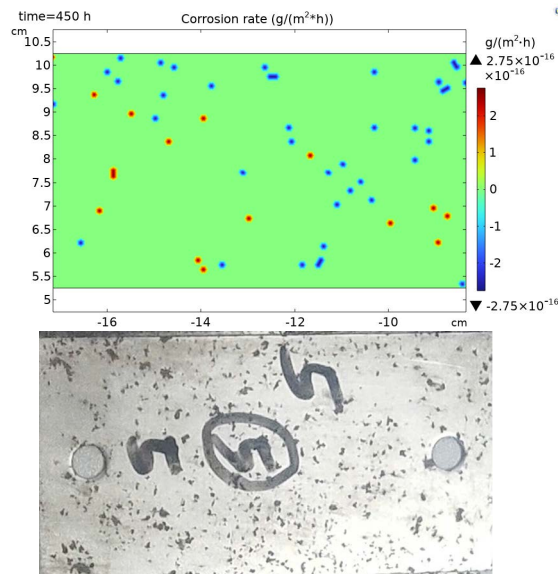
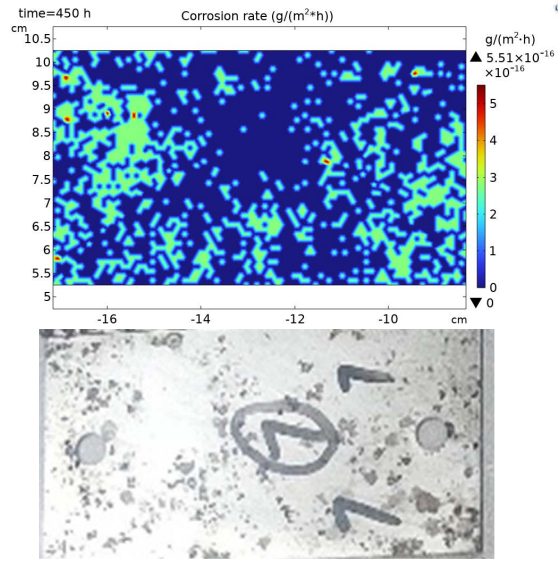(a)   Soil sample added 10 g NaCl

(a) Soil sample added 0 g NaCl
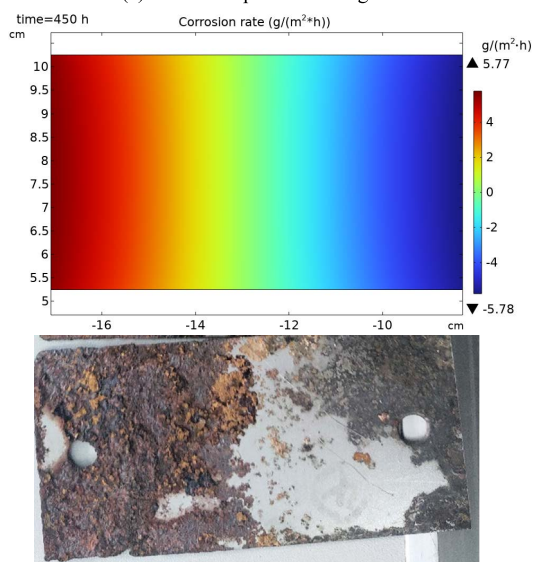
(b) Soil sample added 30 g NaCl

FIGURE 12. Contrast results of experimental group.

(b)Soil sample added 20 g NaCl

FIGURE 13. Contrast results of control group.

corrosion phenomenon. Moreover, the corrosion degree and corrosion rate of carbon steel sheets also increase with the increase of soil salt content. However, the degree of corrosion is relatively small, and only a slight corrosion phenomenon occurs.

The results of the experimental group and the control group are analyzed, it can be found that the corrosion degree and the corrosion rate of the buried carbon steel sheets will be significantly increased when there is an external power supply. 20 g NaCl added in the soil is taken as an example, in the experiment, the corrosion rate reaches 0.11652 g/day when there is an external voltage, but only 0.02142g/day when there is no external voltage. In the simulation, when the time set at 450 h, the maximum corrosion rate with external voltage reaches $5.76 \, g/\left(m^2 \cdot h\right)$, while the maximum

corrosion rate without external voltage is only $5.51 \times 10^{-16} \times 10^{-16} \, g/\left(m^2 \cdot h\right)$.

VI. CONCLUSION

In this paper, a small experimental platform for the corrosionof the buried metals by DC stray current is firstly built. By measuring and calculating the corrosion rate and the mass loss of the buried carbon steel sheets in soil samples with or without DC stray current, the influence of soil salt content on the corrosion of the buried metal is studied. And the accuracy of the experimental results is verified by establishing a multiphysics simulation model corresponding to the experiment. Therefore, the following conclusions can be drawn. Firstly, the corrosion rate and the mass loss of buried metals increase with the increase of soil salt content.

Secondly, DC stray current will aggravate the corrosion of the buried metals. Thirdly, the corrosion degree of buried metal will be seriously aggravated under the coupling action of the DC stray current and salt. Fourthly, when there is no DC stray current, the corrosion degree of the buried metal is relatively small, and the influence of soil salt content is also relatively small.

CONFLICTS OF INTEREST
The authors declare no conflict of interest.

DATA AVAILABILITY
The data that support the findings of this study are available from the corresponding author upon reasonable request.

REFERENCES

[1] B. M. Han and F. Lu, "Statistical analysis of urban rail transit operations in the world in 2021: A review," *Urban Rapid Rail Transit*, vol. 35, no. 1, pp. 5–11, Jan. 2021, doi: 10.3969/j.issn.1672-6073.2022.01.002.

[2] A. Wang, S. Lin, Z. Hu, J. Li, F. Wang, G. Wu, and Z. He, "Evaluation model of DC current distribution in AC power systems caused by stray current of DC metro systems," *IEEE Trans. Power Del.*, vol. 36, no. 1, pp. 114–123, Feb. 2021, doi: 10.1109/TPWRD.2020.2975367.

[3] W. Liu, "Measurement method and calculation error of rail-to-earth resistance in urban rail," *High Voltage Eng.*, vol. 46, no. 8, pp. 2856–2863, Aug. 2020, doi: 10.13336/j.1003-6520.hve.20190147.

[4] Y. J. Hu, Z. Zhong, and J. P. Fang, "Finite element simulation of subway stray current field," *China Railway Sci.*, vol. 32, no. 6, Nov. 2011, pp. 129–133.

[5] F. Zhu, J. G. Wang, H. Zeng, and R. Qiu, "Influence of Rail-to-ground resistance of urban transit systems on distribution characteristics of stray current," *High Voltage Eng.*, vol. 44, no. 8, pp. 2738–2745, Aug. 2018, doi: 10.13336/j.1003-6520.hve.20180731034.

[6] A. Wang, S. Lin, J. Li, and Z. He, "Stray current simulation model of the long line of DC metro systems," *High Voltage Eng.*, vol. 46, no. 46, pp. 1379–1386, 2020, doi: 10.13336/j.1003-6520.hve.20200430030.A.

[7] S. Lin, Q. Zhou, X. Lin, M. Liu, and A. Wang, "Infinitesimal method based calculation of metro stray current in multiple power supply sections," *IEEE Access*, vol. 8, pp. 96581–96591, 2020, doi: 10.1109/ACCESS.2020.2994125.

[8] C. Wang, W. Li, Y. Wang, S. Xu, and K. Li, "Evaluation model for the scope of DC interference generated by stray currents in light rail systems," *Energies*, vol. 12, no. 4, p. 746, Feb. 2019, doi: 10.3390/en12040746.

[9] L. Cai, J. G. Wang, Y. D. Fan, M. Zhou, M. R. Gong, and S. W. Liu, "Influence of the track-to-earth resistance of subway on stray current distribution," *High Voltage Eng.*, vol. 41, no. 11, pp. 3604–3610, Nov. 2015, doi: 10.13336/j.1003-6520.hve.2015.11.012.

[10] S.-Y. Xu, W. Li, and Y.-Q. Wang, "Effects of vehicle running mode on rail potential and stray current in DC mass transit systems," *IEEE Trans. Veh. Technol.*, vol. 62, no. 8, pp. 3569–3580, Oct. 2013, doi: 10.1109/TVT.2013.2265093.

[11] T. Eichler and B. Isecke, "Stray current-induced corrosion in cathodic protection installations of steel-reinforced concrete structures: FEM study of the critical parameters," *Mater. Corrosion*, vol. 71, no. 5, pp. 738–748, May 2020, doi: 10.1002/maco.202011620.

[12] A. Ogunsola, A. Mariscotti, and L. Sandrolini, "Estimation of stray current from a DC-electrified railway and impressed potential on a buried pipe," *IEEE Trans. Power Del.*, vol. 27, no. 4, pp. 2238–2246, Oct. 2012, doi: 10.1109/TPWRD.2012.2211623.

[13] K. Tang, "Stray current induced corrosion of steel fibre reinforced concrete," *Cement Concrete Res.*, vol. 100, pp. 445–456, Oct. 2017, doi: 10.1016/j.cemconres.2017.08.004.

[14] Z. Cai, X. Zhang, and H. Cheng, "Evaluation of DC-subway stray current corrosion with integrated multi-physical modeling and electrochemical analysis," *IEEE Access*, vol. 7, pp. 168404–168411, 2019, doi: 10.1109/ACCESS.2019.2953960.

[15] H. Jin and S. Yu, "Effect of DC stray current on rebar corrosion in cracked segment of shield tunnel," *Construct. Building Mater.*, vol. 272, Feb. 2021, Art. no. 121646, doi: 10.1016/j.conbuildmat.2020.121646.

[16] X. Peng, Z. Huang, B. Chen, D. Liu, and H. Li, "On the interference mechanism of stray current generated by DC tram on pipeline corrosion," *Eng. Failure Anal.*, vol. 116, Oct. 2020, Art. no. 104760, doi: 10.1016/j.engfailanal.2020.104760.

[17] Z. Chen, L. Gao, and D. A. Koleva, "Evaluating the stray current corrosion of steel rebar in different layouts," *Measurement*, vol. 196, Jun. 2022, Art. no. 111217, doi: 10.1016/j.measurement.2022.111217.

[18] J. Shi, Y. Zou, J. Ming, and M. Wu, "Effect of DC stray current on electrochemical behavior of low-carbon steel and 10%Cr steel in saturated $Ca(OH)_2$ solution," *Corrosion Sci.*, vol. 169, Jun. 2020, Art. no. 108610, doi: 10.1016/j.corsci.2020.108610.

[19] Z. Zhu, C. Shi, Y. Zhang, and Z. Liu, "The effects of Cl^- and direct stray current on soil corrosion of three grounding grid materials," *Anti-Corrosion Methods Mater.*, vol. 67, no. 1, pp. 73–82, Jan. 2020, doi: 10.1108/ACMM-06-2019-2136.

[20] Z. P. Chen, and, and D. A. Koleva, "Corrosion behavior of reinforcing steel undergoing stray current and anodic polarization," *Materials*, vol. 14, no. 2, pp. 1–23, Jan. 2021, doi: 10.3390/ma14020261.

[21] C. T. Wang, W. Li, and Y. Q. Wang, "Remaining lifetime assessment of gas pipelines subjected to stray current interference using an integrated electric-electrochemical method," *Eng. Failure Anal.*, vol. 127, pp. 1–15, May 2021, doi: 10.1016/j.engfailanal.2021.105494.

[22] X. Liu, M. Xia, D. Bolati, J. Liu, Q. Zheng, and H. Zhang, "An ANN-based failure pressure prediction method for buried high-strength pipes with stray current corrosion defect," *Energy Sci. Eng.*, vol. 8, no. 1, pp. 248–259, Jan. 2020, doi: 10.1002/ese3.522.

[23] Y. Hong, Z. Li, G. Qiao, and J. Ou, "Numerical simulation and experimental investigation of the stray current corrosion of viaducts in the high-speed rail transit system," *Construct. Building Mater.*, vol. 157, pp. 416–423, Dec. 2017, doi: 10.1016/j.conbuildmat.2017.09.114.

[24] H. X. Wan, T. T. Li, D. D. Song, and C. F. Chen, "Research progress of stray current on corrosion and drainage method of buried pipeline," *Surf. Technol.*, vol. 50, no. 4, pp. 125–134, Apr. 2021, doi: 10.16490/j.cnki.issn.1001-3660.2021.04.012.

[25] C. T. Wang, W. Li, G. F. Xin, Y. Q. Wang, X. F. Yang, and Z. A. Guo, "Experimental research examining the stray current corrosion of rock bolts in the DC transit system," *Experim. Techn.*, vol. 44, no. 2, pp. 137–148, Apr. 2020, doi: 10.1007/s40799-019-00343-x.

[26] J. Q. Zhang, J. N. Zhang, H. D. Yang, Y. H. Wu, and W. H. Li, "Research on the relationship between conductivity and salinity content of soil in suburb of Lanzhou," *J. Gansu Sci. Technol.*, vol. 34, no. 2, pp. 2738–2745, Jun. 2009.

[27] Y. Li, M. Jiao, and Y. Wang, "Effect of soil salt content on stray current distribution in urban rail transit," *IEEE Access*, vol. 9, pp. 168433–168443, 2021, doi: 10.1109/ACCESS.2021.3132630.

YANING LI is currently an Associate Professor. She is also a Master Tutor with the School of Automation and Electrical Engineering, Lanzhou Jiaotong University. Her research interests include urban rail transit power supply systems, stray current, corrosion, and photovoltaic power generation.

MENG JIAO is currently pursuing the master's degree with Lanzhou Jiaotong University, China. Her research interests include metro stray current, corrosion, and grounding technology.

HONG KANG is currently pursuing the master's degree with Lanzhou Jiaotong University, China. His research interests include metro stray current, traction energy consumption, and stray current.

YE WANG is currently a Professor. He is also a Doctoral Tutor with the School of Environment and Municipal Engineering, Lanzhou Jiaotong University. He is a Peer Review Expert of NSFC, a Communication Review Expert of degree center of Ministry of Education, and a reviewer of many important domestic journals. His research interests include natural convection, heat transfer enhancement, and engineering application.

WENFEI LI received the master's degree from Lanzhou Jiaotong University. His research direction in school is the distribution and influencing factors of stray current in urban rail transit.

WENCAI ZHANG is currently pursuing the master's degree with Lanzhou Jiaotong University, China. His research interests include metro stray current, traction energy consumption, and stray current.

● ● ●